Journal of Applied Electrochemistry (2020) 50:71–79
https://doi.org/10.1007/s10800-019-01366-3

RESEARCH ARTICLE

One-step hydrothermal synthesis of GQDs-MoS_2 nanocomposite with enhanced supercapacitive performance

Sara Moghimian[1] · Parvaneh Sangpour[1]

Received: 8 June 2019 / Accepted: 24 October 2019 / Published online: 6 November 2019

Abstract

In recent years, graphene quantum dots with unique physiochemical properties have received considerable research attention in many fields. In this report, as a novel approach toward improving the capacitance value of MoS_2 electrode, GQDs-MoS_2 nanocomposite thin film was synthesized through one-step hydrothermal process. The microstructure and surface morphology of both MoS_2 and GQDs-MoS_2 nanocomposite thin films were characterized by X-ray diffraction, Raman spectroscopy, field emission-scanning electron microscopy, and Fourier transform infrared spectroscopy. The electrochemical performances of MoS_2 and GQDs-MoS_2 nanocomposite thin films was thoroughly compared via Autolab potentiostat–galvanostat with the three-electrode system. The results indicated that GQDs-MoS_2 nanocomposite thin film demonstrates enhanced specific capacitance of 380 F g^{-1} under the current density of 0.6 A g^{-1}. Moreover, the MoS_2-GQDs thin film exhibited the highest energy density of 38.47 Wh kg^{-1} at the Current density of 0.6 A g^{-1}.

Graphic abstract

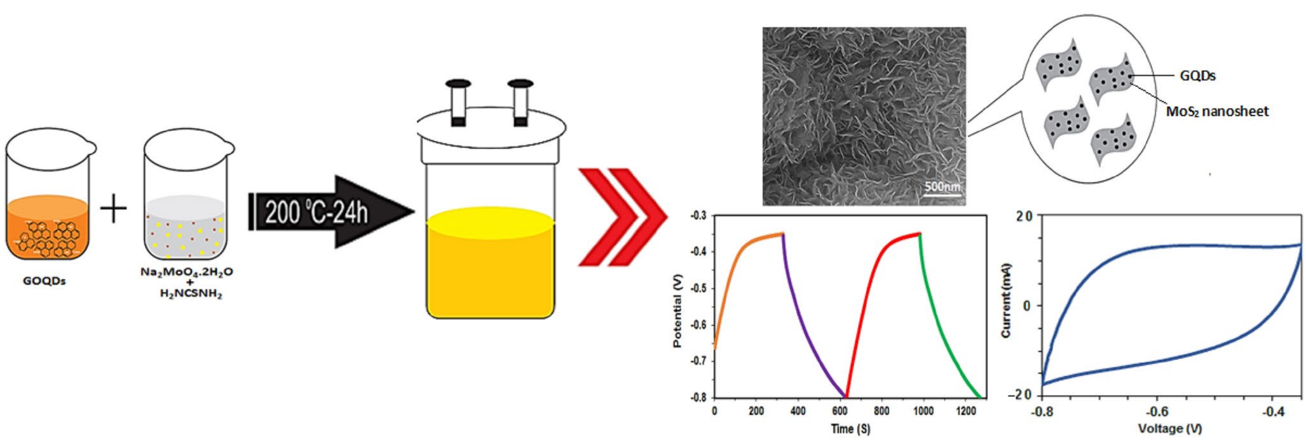

Keywords Graphene quantum dots · Nanocomposite · Electrochemical performance · Supercapacitors

1 Introduction

The excessive use of fossil fuels and the continuous increase of greenhouse gasses have been accelerating the demand for more efficient and environmentally friendly energy generation and storage devices [1, 2]. Numerous research has been focused on the development of advanced materials for energy storage [3–7]. Energy storage devices with high energy and power density possess potential applications in

Electronic supplementary material The online version of this article (https://doi.org/10.1007/s10800-019-01366-3) contains supplementary material, which is available to authorized users.

✉ Parvaneh Sangpour
sangpour@merc.ac.ir

[1] Department of Nanotechnology and Advanced Materials, Materials and Energy Research Centre, P.O. Box 31787-316, Karaj, Iran

portable electronics, memory backup systems, electric vehicles, and industrial power systems [8–12].

Supercapacitors, namely electrochemical capacitors (ECs), are one of the energy storage devices that have attracted significant attention in recent years [13–16]. The major reason is that in comparison with other energy storage devices such as batteries, they possess a higher power density, longer cycle life, and a faster charge–discharge [17, 18]. However, suffering from low-energy density and low-voltage per cell, their applications have been restricted in many fields. Therefore, considerable efforts have been made to improve the components of supercapacitors such as electrolytes, binders, and especially electrode materials [19–23]. In general, depending on the mechanism of charge storage, supercapacitors can be divided into two major groups; pseudocapacitor (PCs) and electrical double-layer capacitor (EDLCs) [21, 23–25]. While the charge storage in EDLC is based on ion intercalation–deintercalation at the electrode–electrolyte interface and popular electrode materials are carbon-based components, PCs is achieved by Faradaic reaction and the most common electrode materials are metal oxides, transition metal dichalcogenides (TMDs) and conductive polymers [25–29].

Molybdenum disulfide (MoS_2) is one of the TMD materials with a layered S-Mo-S structure S and analogous to graphite [30]. Due to excellent physical and chemical properties, it has attracted considerable interests in many fields such as catalyst [31, 32], electrochemical devices [33–35], electronic and photonics [36–38], batteries [39–41], and hydrogen storage [42, 43]. MoS_2 has also considered as a one of the potential electrode materials for supercapacitors because of its intrinsic high-theoretical capacity [44–49]. However, like other supercapacitors, it suffers from low-specific energy density [46, 48]. Generally, to increase the energy density of supercapacitors, major approaches such as increasing the specific capacity of the electrode materials or using electrolytes with wider potential windows have been taken. For example, regarding the enhanced specific capacitance of MoS_2, the combination of MoS_2 with conductive additives such as activated carbon, graphene composites, and metal oxides has been introduced as a favorable approach. [48, 50, 51].

In recent years, graphene quantum dots (GQDs) as a new carbon-based materials with zero dimension, have received broad research attention in many fields [51–57]. GQDs are small fragments of a single-layer or multi-layer graphene with a small particle size (under 20 nm) [56, 57]. Having fantastic properties such as chemical stability, strong photoluminescence, and high mobility, they are considered as interesting materials for optoelectronics, biological and environmental applications [53–56]. Moreover, owing to good electrical conductivity and high-surface area, they are suitable candidates for energy storage and conversion; photovoltaic cells, rechargeable batteries and supercapacitors [58–61]. For example, studies on GQDs/MnO_2 supercapacitor [62], GQDs/polyaniline nanofiber supercapacitor [63], and GQDs–$CuCo_2S_4$ nanocomposites supercapacitor [64] have proved that GQDs can enhance the electrical properties and supercapacitor performance of the electrode materials.

In this work, as a novel approach toward improving the capacitance value of MoS_2, we have investigated the supercapacitor behavior of GQDs-MoS_2 nanocomposite thin film. We fabricated MoS_2-GQDs nanocomposite with the simple hydrothermal method and compared the effect of adding GQD on electrochemical capacitive properties of pure MoS_2. The results indicated that regarding fantastic properties of GQDs, a combination of GQDs and MoS_2 into a single electrode can significantly improve the electrochemical properties and the capacitance behavior of molybdenum disulfide.

2 Experimental

2.1 Materials

Citric acid, sodium hydroxide, sodium molybdate dihydrate, thiourea, carbon black, and polyvinylidene fluoride were purchased from Merck Company and used as received.

2.2 Synthesis methods

MoS_2 was synthesized through the hydrothermal method [65]. GQDs were fabricated using pyrolysis of citric acid as previously reported in the literature [66] (the complete details are available in supporting information).

2.3 Characterization techniques

The microstructure, size distribution, surface morphology and chemistry of the MoS_2 and MoS_2-GQDs composite were characterized using X-ray diffraction (XRD, Philips PW 3710 x-ray diffractometer, with Cu kα radiation), Raman (Thermonicolet, Almega), field emission scanning electron microscopy (FE-SEM, Hitachi S4160), and Fourier transform infrared spectroscopy (FTIR, Perkin Elmer, Spectrum RXI).

2.4 Preparation of electrodes and electrochemical measurement

For the fabrication of working electrodes, the active materials, carbon black, and polyvinylidene fluoride (PVDF) were mixed in the mass ratio of 70:20:10. Subsequently, the resultant slurry was coated onto the steel substrate (1 cmx1 cm), followed by drying at 40 °C for 6 h in a vacuum oven.

The electrochemical measurement was performed using Autolab potentiostat–galvanostat (PGSTAT30) with a three-electrode system, containing Ag/AgCl as the reference electrode and a platinum wire as the counter electrode. 1 M KOH was selected as the electrolyte solution. The results were analyzed using cyclic voltammetry (CV), galvanostatic charge–discharge (GCD), and electrochemical impedance spectroscopy (EIS). CV tests were carried out between -0.8 and -0.35 V at different scan rates (5, 10, 25, 50, and 100 mV s^{-1}). Galvanostatic charge–discharge was measured at the same potential range for different current densities (0.6, 1 and 2 A g^{-1}). The frequency range for EIS tests was selected from 0.1 Hz to 100 kHz at open circuit potential of 0.46 mV.

3 Results and discussion

3.1 Material characterization

The structural properties of the MoS_2 and MoS_2-GQDs was studied by XRD analysis (Fig. 1). The XRD of the MoS_2 shows obvious peaks at 2θ = 14.3, 33.4, 37.8, 51.4, and 59.2, which are assigned to the (002), (100), (103), (105), and (110), respectively. For the MoS_2-GQDs composite, the extra peak at 2θ = 27.2 related to (002) plane of GQDs. The XRD pattern of GQDs is available in Electronic supporting material.

The Raman spectrum of MoS_2-GQDs composite is shown in Fig. 2. Two major peaks observed at 381 cm^{-1} and 404 cm^{-1} confirm that MoS_2 is successfully fabricated. The first peak is due to the in-plane E^1_{2g} vibration mode and arises from opposite vibration of two S and one M atoms while the A_{1g} mode is related to the out-of-plane vibration of only S atom in opposite directions [30]. The peaks obtained at 1366 cm^{-1} and 1581 cm^{-1} are assigned to the D band and G band of GQD. While the intensity of the G band is associated with the crystalline structure and graphitized carbon,

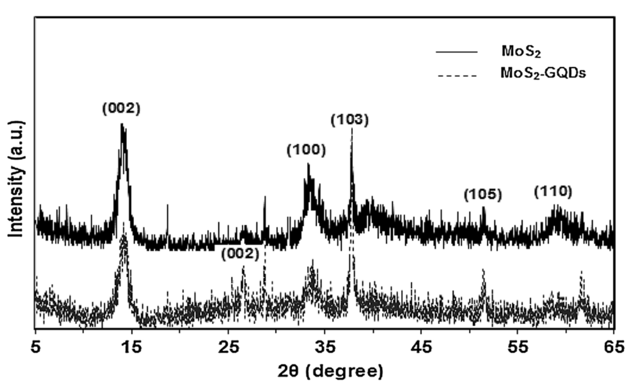

Fig. 1 XRD pattern of MoS_2 and MoS_2-GQDs composite

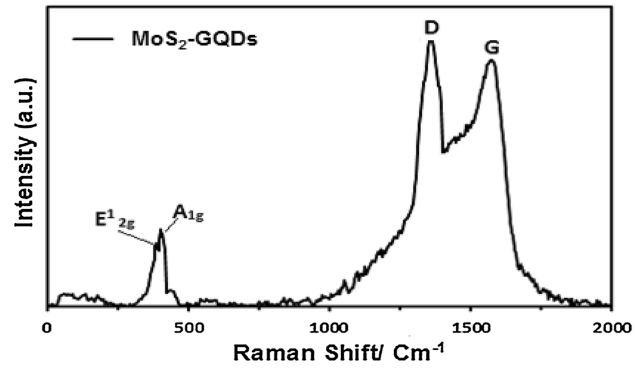

Fig. 2 Raman spectra of MoS_2-GQDs composite

the D band shows the proportion of defects remaining in the structure. Generally, the intensity ratio of the D band to G band (I_D/I_G) is used to characterize the defect quantity in carbon-based materials. The larger ratio of I_D/I_G corresponds to the more disordered carbon atoms, proving the higher disorder structures in the as-prepared GQDs. The ratio of I_D to I_G obtained for the GQDs decorated on MoS_2 is about 1.05, which is higher than some previously reported values [58, 59]. This high- intensity ratio can be related to the small size of GQDs or the effect of abundant edges [58, 59].

The chemical surface of the samples was characterized by FTIR spectra in the range of 4000–500 cm^{-1}. With regard to Fig. 3, the presence of the MoS_2 can be confirmed by the peaks around 3450 and 510 cm^{-1}, related to the OH and Mo-S stretching vibrations [34]. The peak at 3450 cm^{-1} is also observed in MoS_2-GQDs with a bit more intensity, indicating the presence of hydroxyl groups in both MoS_2 and GQDs. Other vibration peaks related to oxygen functional groups of the GQDs are also observed at 1624 and 1108 cm^{-1}, assigning to aromatic C=C vibration and alkoxy C–O–C stretching, respectively. The weak peaks observed in 2919 and 2849 are

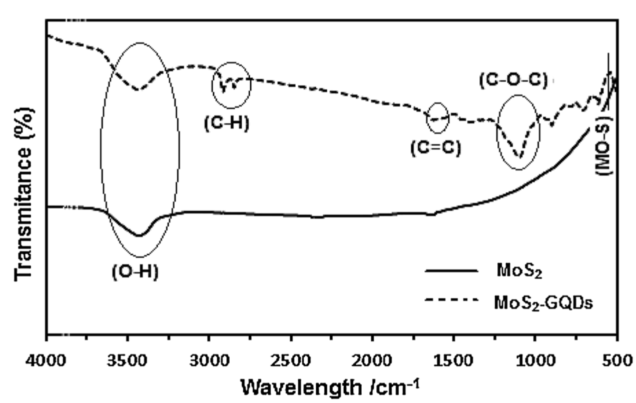

Fig. 3 FTIR spectrum analysis of MoS_2 and MoS_2-GQDs nanocomposite

attributed to the stretching vibration of C–H, indicating that probably citric acid has not entirely carbonized [66]. The morphology and the element distribution of MoS_2 and MoS_2-GQDs nanocomposite are shown by FESEM images and energy-dispersive X-ray spectroscopy (EDS) mapping in Fig. 4. Figure 4a shows the size distribution and formation of prepared GQDs from pyrolysis of citric acid. The average diameter of GQDs nanoparticles is less than 20 nm. The as-prepared MoS_2 exhibits nanosheet structure, which has horizontally compressed on the surface (Fig. 4b). In Fig. 4c, the orientation of MoS_2-GQDs structure is different from pristine MoS_2, composing of small interwoven nanosheets grown vertically on the surface. This structure provides a larger surface area and porosity which facilitate ion diffusion paths. The average thicknesses of layers are around 15 nm, implying the restacking of few-layered during the centrifugation and drying processes. The EDS mapping of the MoS_2-GQDs cross-section proves that GQDs decorated on the basal planes of interwoven nanosheets of MoS_2, showing a uniform hybrid of MoS_2 and GQDs in this section. Moreover, the EDS spectrum of the nanocomposite cross-section reveals that the distribution of Mo, S, C, and O elements are around 40 wt%, 17 wt%, 35 wt%, 7.5 wt% respectively.

3.2 Electrochemical characterization

Capacitive performance of MoS_2 and MoS_2-GQDs electrodes evaluated by cyclic voltammetry (CV) and galvanostatic charge–discharge (GCD) methods using three-electrode systems. Cyclic voltammetry and charge–discharge tests were performed in aqueous 1 M KOH solution at different scan rates and current densities. Figure 5a, b compare the CV curves of both electrodes at various scan rates, from 5 mV s^{-1} to 100 mV s^{-1}. For both electrodes, the shapes of the CVs are almost rectangular and without any redox peaks, meaning that the charge storage is based on ion intercalation–deintercalation at the electrode–electrolyte interface and the electrodes present EDLC behavior. With increasing the scan rates, the current response increased and the CV curves maintained their quasi-rectangular shapes. This indicates that not only at lower scan rates but also at higher ones rapid and reversible charge transfer can occur at the electrode–electrolyte interface.

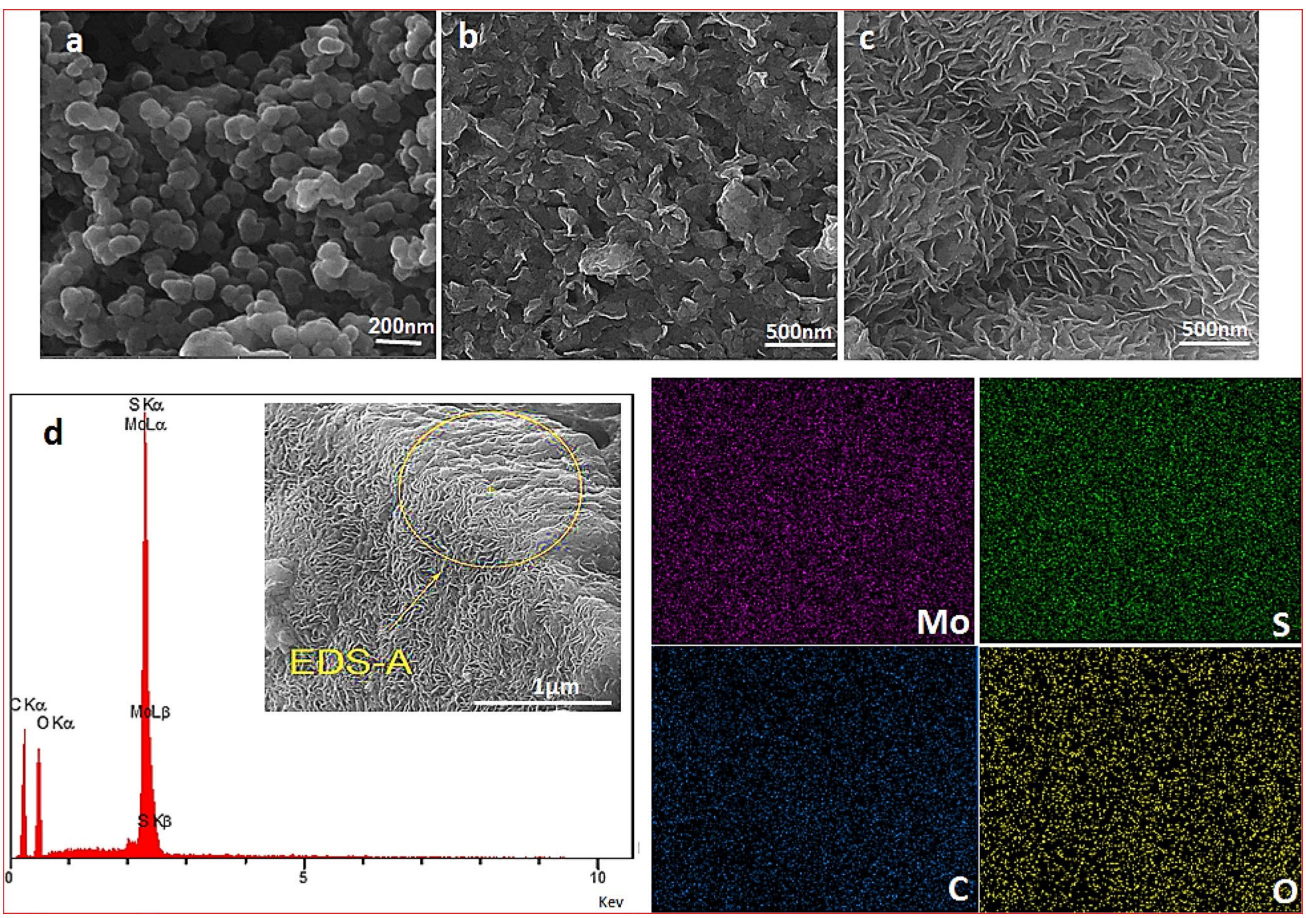

Fig. 4 SEM image of **a** as-prepared GQDs, **b** MoS_2, **c** MoS_2-GQDs nanocomposite, **d** EDS spectrum and maps of MoS_2-GQDs cross-section

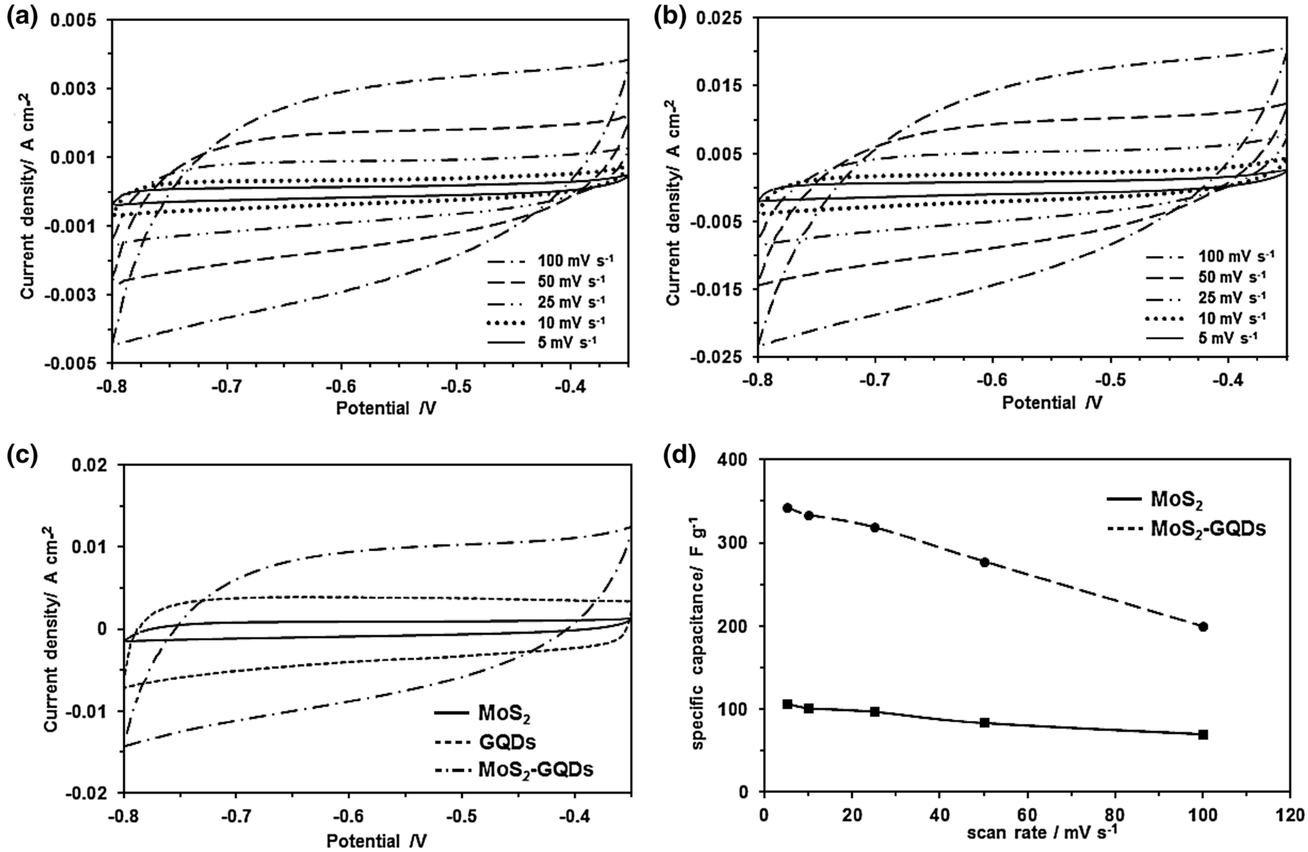

Fig. 5 **a** CV curves of MoS_2 at different scan rates, **b** CV curves of MoS_2-GQDs at different scan rates. **c** Comparison between CV curves of GQDs, MoS_2 and MoS_2-GQDs electrodes at a scan rate of 100 mV s^{-1}, **d** SCs of MoS_2 and MoS_2-GQDs composite at different scan rates

The comparison between CV curves of GQDs, MoS_2, and MoS_2-GQDs electrodes at the scan rate of 100 mV s^{-1} is shown in Fig. 5c. It is clear that in comparison with MoS_2, the CV curves of GQDs and MoS_2-GQDs showed better rectangular shape, higher current densities and larger voltammogram areas, implying that GQDs play a significant role in the enhancing areal capacitance of MoS_2.

From the voltammograms, the specific capacitance (SC) of the electrodes was determined using Eq. 1, in which $\int$I dV is the area under the CV curve, υ is the scan rate, m is the mass of the active material (g), and ΔV is the potential window.

$$SC = \int Idv/vm\Delta V \quad (1)$$

According to Eq. 1, the SC of the MoS_2 electrode was calculated to be 107.3, 101.9, 97.4, 88.9, 79.3 Fg^{-1} at the scan rate of 5, 10, 25, 50, and 100 mV s^{-1} respectively. By comparison, the corresponding SCs of MoS_2-GQDs were 342.2, 333.3, 318.5, 277.7, and 212.2, respectively (Fig. 5d). Averagely, the specific capacitance of MoS_2-GQDs electrode was around three times more than pristine MoS_2, which can be attributed to the fact that nanoscale size of GQDs decorated on MoS_2 layers provides high surface area for ion transition and high conductivity between the electrode and the electrolyte.

The galvanostatic charge–discharge test was investigated in the potential range of −0.8 to −0.35 V at three different current densities (0.6, 1, 2 A g^{-1}). As seen in Fig. 6, the charge–discharge curves of both electrodes have nearly linear shapes in all current ranges, meaning that the electrodes represent the behavior of an ideal capacitor [67]. Additionally, in the initial part of the discharge curve, no clear IR drop is observed for MoS_2-GQDs, which refers to the small internal resistance of the electrode. Regarding charge–discharge time, noticeable differences between both electrodes are observed. For example, the maximum time for the charge and discharge of MoS_2-GQDs electrode at the current density of 1 A g^{-1} is around 182 s and 158 s, which is significantly higher than MoS_2. The improved charge–discharge time of the MoS_2-GQDs can be attributed to the incorporation of the GQDs on the MoS_2 surface. The main reason is that GQDs with the small size and the edge effect supply high electrochemical activity and high surface area for ions intercalation–deintercalation in the composite electrode

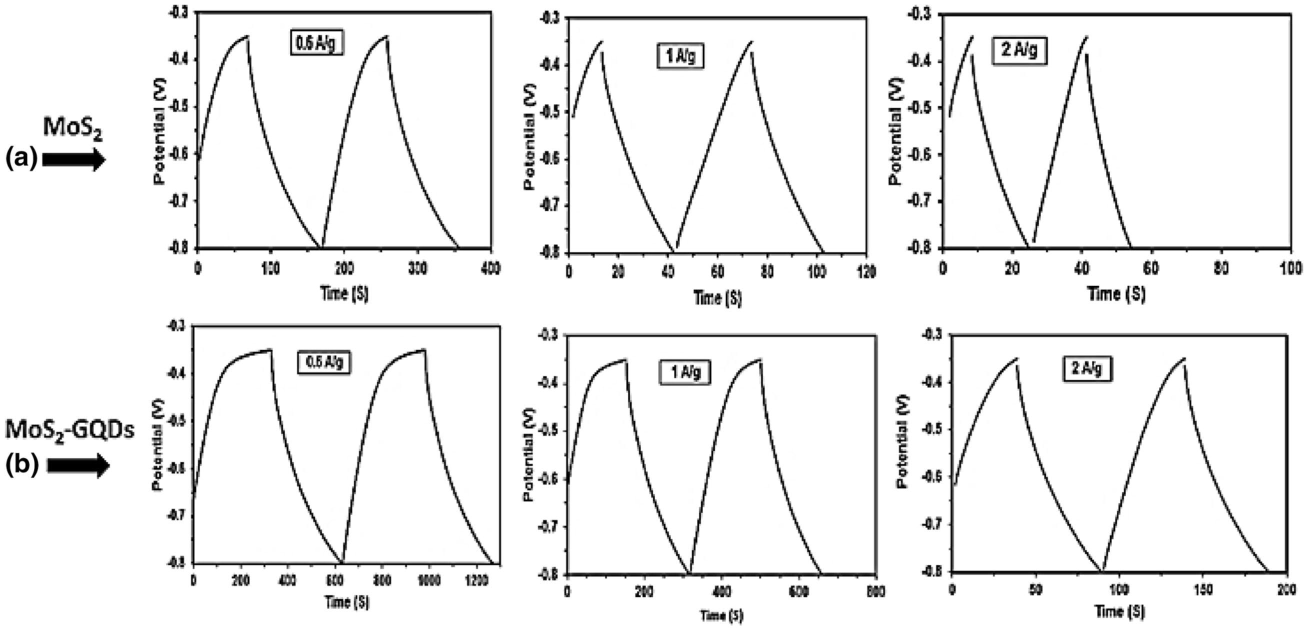

Fig. 6 GCD curves of **a** MoS_2 and **b** MoS_2-GQDs at different current densities

[66]. The specific capacitance of electrodes was also calculated from the galvanostatic charge–discharge cycle. Using Eq. 2, the specific capacitance of the composite electrode was 380.5, 323.5, 221.7 F g^{-1} at a current density of 0.6, 1, and 2 A g^{-1}, respectively. This values are higher than those measured for MoS_2, and are in good agreement with CVs measurement.

$$SC = I\Delta t/m\Delta V \tag{2}$$

As a result, compared to the MoS_2 thin film, the MoS_2-GQDs electrode presents a better discharge time and a higher capacitance value. Interestingly, the specific capacitance value of the MoS_2-GQD is significantly higher than some previous investigation on supercapacitor performance of MoS_2 or graphene-based composites (Table 1).

The energy density (E) and power density (P) are calculated according to the Eqs. (2) and (3), respectively. In these equations SC is the specific capacitance (F g $^{-1}$), ΔV is the voltage range of charge and discharge, and Δt is discharge time.

$$E = SC\Delta V^2/2 \tag{3}$$

$$P = E/\Delta t \tag{4}$$

The MoS_2-GQDs exhibits the highest energy density of 38.47 Wh kg^{-1} at the power density of 486.96 W kg^{-1}. This result proves that the MoS_2-GQD could potentially be considered as electrode materials with high-capacitive performance.

The cyclic stability of the MoS_2-GQDs was tested by 500 continuous cycles, and GCD measurements were carried out at a current density of 3 A g^{-1} (Fig. 7). The specific capacitance of the MoS_2-GQDs composite remained at approximately 92.3% of the initial cycle after 500 cycles.

Table 1 the comparison between some electrode materials based on MoS_2 or GQDs with high-specific capacitance

Electrode materials	SC (F g^{-1})	Current density (A g^{-1})	References
GQDs-MoS_2 nanocomposite	380.5/323.5	0.6/1	This work
Graphene quantum dots	296.7	1	[59]
Molybdenum disulfide-reduced graphene oxide-polyaniline	570	1	[44]
MoS_2–rGO hetrostructure	387.6	2.1	[68]
MoS_2/graphene nanosheets	320	2	[69]
Graphene decorated with MoS_2 nanosheets	270	0.1	[70]
MoS_2 nanosheet arrays-hollow RGO	238	0.5	[49]

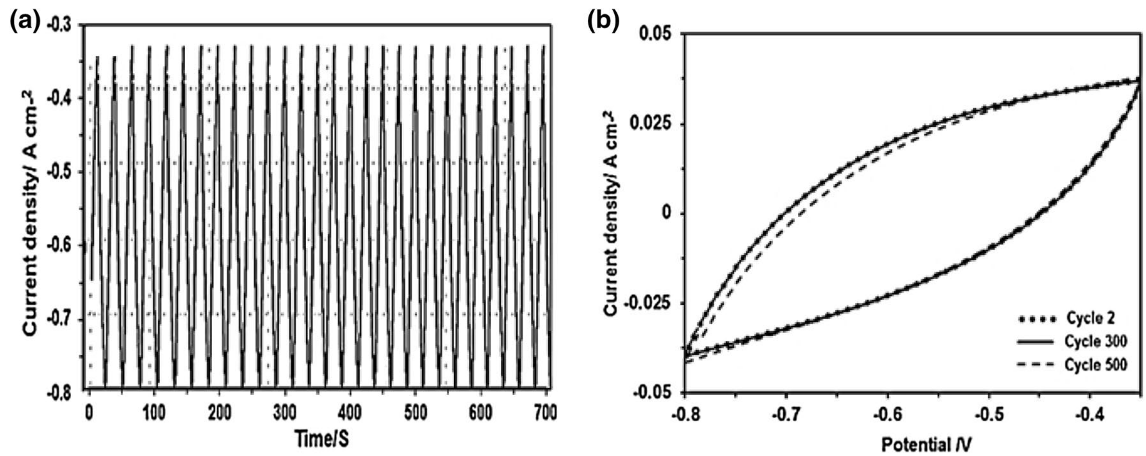

Fig. 7 **a** charge–discharge stability of the MoS_2-GQDs thin film electrode at a current density of 3 A g^{-1} and **b** the cyclic stability of the MoS_2-GQDs electrode at the scan rate of 300 mV s^{-1}

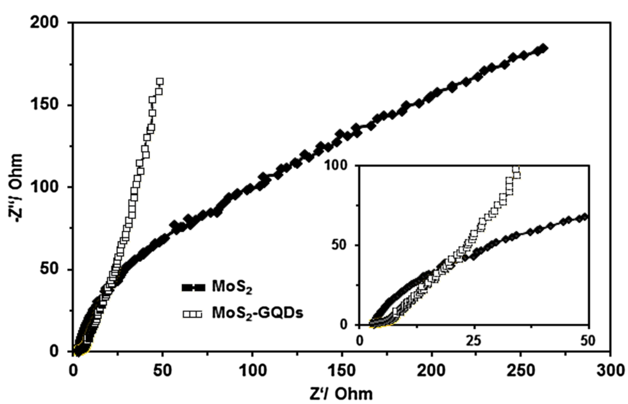

Fig. 8 Nyquist plot of MoS_2 and MoS_2-GQDs

One of the other important methods for the investigation of electrode materials is EIS analysis, which has been illustrated in a frequency range from 10^{-1} to 10^5 Hz (Fig. 8). In high-frequency region, EIS measurements of MoS_2-GQDs did not show a semicircle region in the Nyquist plot, which indicates that the electrode materials have low resistance in the electrolyte and a fast charge transfer occurs between electrode and electrolyte. In addition, the straight line nearly parallels to a vertical axis with a slope of over 45° in a low-frequency region suggesting the presence of GQDs decreases the electrochemical impedance and enhances an ideal capacitive behavior of MoS_2-GQD electrode. In comparison, for the MoS_2 electrode, the approximate semicircle observed in high frequency and the deviation of a straight line in low frequency indicate a higher solution resistance and larger ion diffusion resistance, respectively [67].

4 Conclusion

In conclusion, MoS_2-GQD nanocomposite thin film was simply prepared by one-step hydrothermal method. The surface chemistry of MoS_2-GQD nanocomposite proved that it is comprised of interwoven nanosheets with the average thicknesses of 15 nm, decorated with GQDs on basal planes. The electrochemical measurement exhibited that addition of GQDs leads to improved conductivity, enhanced capacitance and better cycling stability of the pure MoS_2 electrode. Results confirm that GQDs hold great promise in electrochemical applications and continue to be productive for further investigations in energy storage devices.

References

1. Jang BZ et al (2011) Graphene surface-enabled lithium ion-exchanging cells: next-generation high-power energy storage devices. Nano Lett 11(9):3785–3791
2. Zhao X et al (2011) The role of nanomaterials in redox-based supercapacitors for next generation energy storage devices. Nanoscale 3(3):839–855
3. Arico AS et al (2005) Nanostructured materials for advanced energy conversion and storage devices. Nat Mater 4(5):366–377
4. Guan C, Wang J (2016) Recent development of advanced electrode materials by atomic layer deposition for electrochemical energy storage. Adv Sci 3(10):1500405
5. Liu C et al (2010) Advanced materials for energy storage. Adv Mater 22(8):E28–E62
6. Liu J et al (2018) Advanced energy storage devices: basic principles, analytical methods, and rational materials design. Adv Sci 5(1):1700322
7. Han S et al (2014) Porous graphene materials for advanced electrochemical energy storage and conversion devices. Adv Mater 26(6):849–864
8. Chang X et al (2018) Efficient synthesis of tungsten oxide hydrate-based nanocomposites for applications in bifunctional

electrochromic-energy storage devices. Nanotechnology 29(18):185707
9. Gao MR et al (2013) Nanostructured metal chalcogenides: synthesis, modification, and applications in energy conversion and storage devices. Chem Soc Rev 42(7):2986–3017
10. Wei D et al (2012) Graphene from electrochemical exfoliation and its direct applications in enhanced energy storage devices. Chem Commun 48(9):1239–1241
11. Lee H et al (2018) Enhanced electrochemical performance of carbon nanotube with nitrogen and iron using liquid phase plasma process for supercapacitor applications. Int J Mol Sci 19(12):3830
12. Xia H, Xu Q, Zhang J (2018) Recent progress on two-dimensional nanoflake ensembles for energy storage applications. Nanomicro Lett 10(4):66
13. Hu X et al (2019) An advanced NiCoFeO/polyaniline composite for high-performance supercapacitor. Chem Asian J 14(7):977–985
14. Lim E et al (2014) Advanced hybrid supercapacitor based on a mesoporous niobium pentoxide/carbon as high-performance anode. ACS Nano 8(9):8968–8978
15. Moussa M et al (2016) Recent progress and performance evaluation for polyaniline/graphene nanocomposites as supercapacitor electrodes. Nanotechnology 27(44):442001
16. Zuo W et al (2017) Battery-supercapacitor hybrid devices: recent progress and future prospects. Adv Sci 4(7):1600539
17. Mohammed AA, Chen C, Zhu Z (2019) Low-cost, high-performance supercapacitor based on activated carbon electrode materials derived from baobab fruit shells. J Colloid Interface Sci 538:308–319
18. Wang G, Zhang L, Zhang J (2012) A review of electrode materials for electrochemical supercapacitors. Chem Soc Rev 41(2):797–828
19. Galhena DTL et al (2018) Reduced graphene oxide as a monolithic multifunctional conductive binder for activated carbon supercapacitors. ACS Omega 3(8):9246–9255
20. Li Q et al (2018) Recent progress in some amorphous materials for supercapacitors. Small 14(28):e1800426
21. Li Q et al (2019) All hierarchical core-shell heterostructures as novel binder-free electrode materials for ultrahigh-energy-density wearable asymmetric supercapacitors. Adv Sci 6(2):1801379
22. Naderi L, Shahrokhian S (2019) Nickel molybdate nanorods supported on three-dimensional, porous nickel film coated on copper wire as an advanced binder-free electrode for flexible wire-type asymmetric micro-supercapacitors with enhanced electrochemical performances. J Colloid Interface Sci 542:325–338
23. Shi Y et al (2018) Stretchable and self-healing integrated all-gel-state supercapacitors enabled by a notch-insensitive supramolecular hydrogel electrolyte. ACS Appl Mater Interfaces 10(42):36028–36036
24. Muller GA et al (2015) High performance pseudocapacitor based on 2D layered metal chalcogenide nanocrystals. Nano Lett 15(3):1911–1917
25. Zhang X et al (2011) High-power and high-energy-density flexible pseudocapacitor electrodes made from porous CuO nanobelts and single-walled carbon nanotubes. ACS Nano 5(3):2013–2019
26. Sheberla D et al (2017) Conductive MOF electrodes for stable supercapacitors with high areal capacitance. Nat Mater 16:220–224
27. Wang Y, Xia Y (2013) Recent progress in supercapacitors: from materials design to system construction. Adv Mater 25(37):5336–5342
28. Zhang LL, Zhao XS (2009) Carbon-based materials as supercapacitor electrodes. Chem Soc Rev 38(9):2520–2531
29. Zhou Y et al (2016) In-situ fabrication of graphene oxide hybrid Ni-based metal-organic framework (Ni-MOFs@GO) with ultrahigh capacitance as electrochemical pseudocapacitor materials. ACS Appl Mater Interfaces 8(42):28904–28916
30. Li X, Zhu H (2015) Two-dimensional MoS2: properties, preparation, and applications. J Mater 1(1):33–44
31. Zhu H et al (2015) When cubic cobalt sulfide meets layered molybdenum disulfide: a core-shell system toward synergetic electrocatalytic water splitting. Adv Mater 27(32):4752–4759
32. Abbasi P et al (2017) Tailoring the edge structure of molybdenum disulfide toward electrocatalytic reduction of carbon dioxide. ACS Nano 11(1):453–460
33. Zhu G et al (2016) Tuning thermal conductivity in molybdenum disulfide by electrochemical intercalation. Nat Commun 7:13211
34. Winchester A et al (2014) Electrochemical characterization of liquid phase exfoliated two-dimensional layers of molybdenum disulfide. ACS Appl Mater Interfaces 6(3):2125–2130
35. Acerce M, Akdogan EK, Chhowalla M (2017) Metallic molybdenum disulfide nanosheet-based electrochemical actuators. Nature 549(7672):370–373
36. Alrasheed A et al (2018) Surface properties of laser-treated molybdenum disulfide nanosheets for optoelectronic applications. ACS Appl Mater Interfaces 10(21):18104–18112
37. Asadi M et al (2016) Cathode based on molybdenum disulfide nanoflakes for lithium-oxygen batteries. ACS Nano 10(2):2167–2175
38. Bilgin I et al (2015) Chemical vapor deposition synthesized atomically thin molybdenum disulfide with optoelectronic-grade crystalline quality. ACS Nano 9(9):8822–8832
39. Zhou F et al (2014) Carbon nanofibers decorated with molybdenum disulfide nanosheets: synergistic lithium storage and enhanced electrochemical performance. Angew Chem Int Ed Engl 53(43):11552–11556
40. Han P, Chung SH, Manthiram A (2018) Thin-layered molybdenum disulfide nanoparticles as an effective polysulfide mediator in lithium-sulfur batteries. ACS Appl Mater Interfaces 10(27):23122–23130
41. Ge Y et al (2018) Towards thermally stable high performance lithium-ion batteries: the combination of a phosphonium cation ionic liquid and a 3D porous molybdenum disulfide/graphene electrode. Chem Commun 54(42):5338–5341
42. Benson J et al (2015) Electrocatalytic hydrogen evolution reaction on edges of a few layer molybdenum disulfide nanodots. ACS Appl Mater Interfaces 7(25):14113–14122
43. Chen IP et al (2016) Large-scale fabrication of a flexible, highly conductive composite paper based on molybdenum disulfide-Pt nanoparticle-single-walled carbon nanotubes for efficient hydrogen production. Chem Commun 53(2):380–383
44. Bai LZ et al (2018) Synthesis and electrochemical performance of molybdenum disulfide-reduced graphene oxide-polyaniline ternary composites for supercapacitors. Front Chem 6:218
45. Acerce M, Voiry D, Chhowalla M (2015) Metallic 1T phase MoS2 nanosheets as supercapacitor electrode materials. Nat Nanotechnol 10(4):313–318
46. Clerici F et al (2016) In situ MoS_2 decoration of laser-induced graphene as flexible supercapacitor electrodes. ACS Appl Mater Interfaces 8(16):10459–10465
47. Mandal D, Routh P, Nandi AK (2018) Quantum-dot-mediated controlled synthesis of dual oxides of molybdenum from MoS2: quantification of supercapacitor efficacy. Chem Asian J 13(24):3871–3884
48. Wang R et al (2017) Elucidating the intercalation pseudocapacitance mechanism of mos_2-carbon monolayer interoverlapped superstructure: toward high-performance sodium-ion-based hybrid supercapacitor. ACS Appl Mater Interfaces 9(38):32745–32755
49. Zheng S et al (2018) MoS2 nanosheet arrays rooted on hollow rgo spheres as bifunctional hydrogen evolution catalyst and supercapacitor electrode. Nanomicro Lett 10(4):62

50. Yang W et al (2017) Carbon-MEMS-based alternating stacked MoS2@rGO-CNT micro-supercapacitor with high capacitance and energy density. Small 13(26):1700639
51. Liao X et al (2018) MoS_2/MnO_2 heterostructured nanodevices for electrochemical energy storage. Nano Res 11(4):2083–2092
52. Ma CB et al (2015) A general solid-state synthesis of chemically-doped fluorescent graphene quantum dots for bioimaging and optoelectronic applications. Nanoscale 7(22):10162–10169
53. Wang J et al (2016) Synthesis, photoluminescence and bio-targeting applications of blue graphene quantum dots. J Nanosci Nanotechnol 16(4):3457–3467
54. Yan Y et al (2018) Systematic bandgap engineering of graphene quantum dots and applications for photocatalytic water splitting and CO2 reduction. ACS Nano 12(4):3523–3532
55. Zheng P, Wu N (2017) Fluorescence and sensing applications of graphene oxide and graphene quantum dots: a review. Chem Asian J 12(18):2343–2353
56. Zheng XT et al (2015) Glowing graphene quantum dots and carbon dots: properties, syntheses, and biological applications. Small 11(14):1620–1636
57. Zhu S et al (2011) Strongly green-photoluminescent graphene quantum dots for bioimaging applications. Chem Commun 47(24):6858–6860
58. Islam MS et al (2016) In-situ direct grafting of graphene quantum dots onto carbon fibre by low temperature chemical synthesis for high performance flexible fabric supercapacitor. Mater Today Commun 10:112–119
59. Zhang S et al (2018) High-performance supercapacitor of graphene quantum dots with uniform sizes. ACS Appl Mater Interfaces 10(15):12983–12991
60. Zhang J et al (2018) Enhanced performance of planar perovskite solar cell by graphene quantum dot modification. ACS Sustain Chem Eng 6(7):8631–8640
61. Park J et al (2016) Graphene quantum dots: structural integrity and oxygen functional groups for high sulfur/sulfide utilization in lithium sulfur batteries. NPG Asia Mater 8:e272
62. Jia H et al (2018) Heterostructural graphene quantum Dot/MnO_2 nanosheets toward high-potential window electrodes for high-performance supercapacitors. Adv Sci 5(5):1700887
63. Mondal S, Rana U, Malik S (2015) Graphene quantum dot-doped polyaniline nanofiber as high performance supercapacitor electrode materials. Chem Commun 51(62):12365–12368
64. Huang Y et al (2019) Graphene quantum dots-induced morphological changes in $CuCo_2S_4$ nanocomposites for supercapacitor electrodes with enhanced performance. Appl Surf Sci 463:498–503
65. Chang K, Chen W (2011) In situ synthesis of MoS2/graphene nanosheet composites with extraordinarily high electrochemical performance for lithium ion batteries. Chem Commun 47(14):4252–4254
66. Dong YS, Shao J, Chen C, Li H, Wang R, Chi Y, Chen G (2012) Blue luminescent graphene quantum dots and graphene oxide prepared by tuning the carbonization degree of citric acid. Carbon 50(12):4738–4743
67. Liu W et al (2013) Novel and high-performance asymmetric micro-supercapacitors based on graphene quantum dots and polyaniline nanofibers. Nanoscale 5(13):6053–6062
68. Saraf M, Natarajan K, Mobin SM (2018) Emerging robust heterostructure of MoS_2–RGO for high-performance supercapacitors. ACS Appl Mater Interfaces 10(19):16588–16595
69. Yang X et al (2016) A high energy density all-solid-state asymmetric supercapacitor based on MoS_2/graphene nanosheets and MnO_2/graphene hybrid electrodes. J Mater Chem A 4(29):11264–11275
70. Thangappan R et al (2016) Graphene decorated with MoS_2 nanosheets: a synergetic energy storage composite electrode for supercapacitor applications. Dalton Trans 45(6):2637–2646